Cell

Expression Cloning of TMEM16A as a Calcium-Activated Chloride Channel Subunit

Björn Christian Schroeder,[1] Tong Cheng,[1] Yuh Nung Jan,[1] and Lily Yeh Jan[1,*]
[1]Department of Physiology, Howard Hughes Medical Institute, University of California, San Francisco, San Francisco, CA 94143, USA
*Correspondence: lily.jan@ucsf.edu
DOI 10.1016/j.cell.2008.09.003

SUMMARY

Calcium-activated chloride channels (CaCCs) are major regulators of sensory transduction, epithelial secretion, and smooth muscle contraction. Other crucial roles of CaCCs include action potential generation in *Characean* algae and prevention of polyspermia in frog egg membrane. None of the known molecular candidates share properties characteristic of most CaCCs in native cells. Using Axolotl oocytes as an expression system, we have identified TMEM16A as the *Xenopus* oocyte CaCC. The TMEM16 family of "transmembrane proteins with unknown function" is conserved among eukaryotes, with family members linked to tracheomalacia (mouse TMEM16A), *gnathodiaphyseal dysplasia* (human TMEM16E), aberrant X segregation (a *Drosophila* TMEM16 family member), and increased sodium tolerance (yeast TMEM16). Moreover, mouse TMEM16A and TMEM16B yield CaCCs in Axolotl oocytes and mammalian HEK293 cells and recapitulate the broad CaCC expression. The identification of this new family of ion channels may help the development of CaCC modulators for treating diseases including hypertension and cystic fibrosis.

INTRODUCTION

Since the first reports of calcium-activated chloride channels (CaCCs) in salamander photoreceptors (Bader et al., 1982) and *Xenopus* oocytes (Barish, 1983; Miledi, 1982), calcium-activated chloride channels have been implicated in important physiological functions, including the high-gain, low-noise amplification in olfactory transduction, taste adaptation, control of action potential waveform and firing pattern in neurons, membrane potential stabilization in photoreceptors, modulation of fluid secretion from glands and airway epithelia, and positive feedback regulation of smooth muscle contraction induced by G protein-coupled receptors (GPCRs) (Arreola et al., 1995; Hartzell et al., 2005; Nilius et al., 1997). Thus, CaCC blockers may cause vasodilatation (Large and Wang, 1996). Because both CaCCs and cystic fibrosis transmembrane conductance regulator (CFTR) reside on the apical membrane of airway epithelia and regulate airway surface liquid for microbe removal—an essential innate defense mechanism—modulators of CaCC activity have also been considered for the treatment of cystic fibrosis and other pulmonary diseases (Tarran et al., 2006).

CaCCs participate in electrical signaling of a remarkably wide range of eukaryotes, owing to the ubiquity of calcium signaling and the ability of chloride channel activity to influence membrane potential. Not only are CaCCs implicated in the regulation of neuronal excitability in the animal kingdom (Frings et al., 2000), but CaCCs are also important for action potential generation in *Characean* algae and possibly in the sensitive plant, as well (Fromm and Lautner, 2007; Samejima and Sibaoka, 1982).

The hallmark CaCC features, such as voltage dependence of calcium activation and a preference for permeating large anions, are shared by many CaCCs in various cell types, including *Xenopus* oocytes, secretory epithelial cells, hepatocytes, pulmonary artery endothelial cells, and vascular, airway, and gut smooth muscles (Hartzell et al., 2005). Whereas CaCCs are likely activated by direct calcium binding in multiple cell types, such as salivary gland acinar cells and pulmonary endothelial cells, some CaCCs may be stimulated by the calcium-calmodulin-dependent protein kinase CaMKII or other calcium-dependent mechanisms (Hartzell et al., 2005). Although Bestrophin-1, a calcium-activated chloride channel linked to Best vitelliform macular dystrophy (Sun et al., 2002), and Bestrophin-2 may correspond to some epithelial CaCCs (Barro-Soria et al., 2008) and RNAi data support a role for Bestrophin-2 as CaCC in olfactory receptor neurons (Pifferi et al., 2006), none of the molecular candidates of CaCC shows the characteristic voltage dependence at submaximal calcium concentrations but not at high intracellular calcium levels (Pusch, 2004). The question remains whether there are entirely novel CaCCs awaiting molecular characterization (Eggermont, 2004; Hartzell et al., 2005).

Expression cloning has proven useful in identifying new families of ion channels. Unfortunately, the *Xenopus* oocyte is not suitable as an expression system for CaCC expression cloning, owing to its robust CaCC expression, important for generating the fertilization potential after fusion with a sperm cell to prevent polyspermia (Runft et al., 1999). This has further contributed to the frustration in CaCC molecular studies.

In this study, we report expression cloning of the *Xenopus* oocyte CaCC using oocytes from the physiologically polyspermic

Axolotl (*Ambystoma mexicanum*) (Jego et al., 1986) as an expression system, leading to the identification of a novel CaCC subunit as the *Xenopus* TMEM16A (xTMEM16A). The xTMEM16A-induced current resembles the *Xenopus* oocyte CaCC in its anion selectivity, voltage dependence of calcium activation, and sensitivity to several chloride channel blockers. Interestingly, we found that CaCCs endogenous to *Xenopus* oocytes as well as those produced by xTMEM16A in Axolotl oocytes gave rise to multiple current components with different anion selectivity. We further show that two mouse homologs, mouse TMEM16A (mTMEM16A) and mouse TMEM16B (mTMEM16B), also generated CaCCs in Axolotl oocytes. Moreover, mTMEM16A yielded CaCCs in the mammalian HEK293 cells and is broadly expressed in tissues known to contain native CaCCs. In addition to facilitating the identification of CaCC modulators, our finding that the *Xenopus* oocyte CaCC belongs to the evolutionarily conserved TMEM16 family opens the question whether other TMEM16 family members also form anion channels or transporters in mammals and other eukaryotes.

RESULTS

Expression Cloning of *Xenopus* Oocyte CaCC

The robust expression of CaCC endogenous to *Xenopus* oocytes renders this classical expression system unsuitable for CaCC expression cloning. To search for a new expression system, we took into consideration the fact that most salamander species are physiologically polyspermic (Runft et al., 1999) and tested whether Axolotl oocytes that allow multiple sperm entry (Jego et al., 1986) express endogenous CaCCs. We found that these oocytes displayed the voltage-gated proton current as reported previously (Barish and Baud, 1984) (Figure 1A); however, no CaCC current was induced in Axolotl oocytes injected with caged IP_3 and subjected to ultraviolet (UV) flash illumination for photo-release of IP_3 (Figure 1B). To assess Axolotl oocytes as an expression system, we injected cRNA for the small-conductance calcium-activated potassium channel SK2 and found functional expression (Figure 1C).

Next, we examined whether injection of total mRNA from *Xenopus* oocytes could induce CaCCs in Axolotl oocytes. Indeed, robust CaCC current appeared in Axolotl oocytes injected with *Xenopus* oocyte mRNA (Figure 1E) but not water (Figures 1D and 1F) in response to 200 ms UV flash for photo-release of IP_3. It has been shown for the *Xenopus* oocyte CaCC that, whereas short UV flashes induce moderate increase of internal calcium level, resulting in CaCC with pronounced outward rectification, UV flashes of longer duration cause greater calcium elevation and hence nearly linear current-voltage relationship of the CaCC (Callamaras and Parker, 2000) (Figure 1G). We therefore used UV flashes of long duration and monitored IP_3-induced inward current at hyperpolarized membrane potential (Figure 1E) during the course of expression cloning, so as to avoid the confounding contribution of voltage-gated proton channels that are activated upon depolarization (Figure 1A).

For expression cloning, we began by testing size-fractionated *Xenopus* oocyte polyA$^+$ RNA and found that only the ~5–7 kb fraction induced CaCC currents in Axolotl oocytes. We used the oocyte expression vector pBaer6 and inserted cDNA fragments that were larger than 5 kb to generate a directional cDNA library (see the Experimental Procedures). After subdivision of cDNA pools, a single 5191 base pair cDNA clone was found to produce CaCCs (Figures 1F and 1H) with the characteristic voltage dependence. The longest open reading frame, which is preceded by an in-frame stop codon, encodes a protein of 979 amino acids and has a predicted molecular weight of 113 kDa. Database searches identified it as the *Xenopus* ortholog of human and mouse TMEM16A, a member of the TMEM16 family (Figure 1K) estimated to contain six to eight transmembrane segments (Juschke et al., 2005; Tsutsumi et al., 2004). The sequence was deposited in the GenBank database (accession number EU367938).

Functional Expression of xTMEM16A, mTMEM16A, and mTMEM16B in Axolotl Oocytes

Next we cloned mTMEM16A, mTMEM16A with green fluorescence protein (GFP) fused to its C terminus, and mTMEM16B cDNA into oocyte expression vector to test whether the expression of other members of the TMEM16 family also generates calcium-activated chloride currents. Indeed, similar to xTMEM16A (Figure 1H), mTMEM16A, mTMEM16A-GFP (Figure 1I), and mTMEM16B (Figure 1J) also generated CaCCs in Axolotl oocytes that resemble *Xenopus* oocyte CaCCs (Figure 1G).

Voltage-Dependent Calcium Activation of the xTMEM16A-Induced Current

A hallmark feature of CaCCs in many native cells including *Xenopus* oocytes is the strong outward rectification at submaximal calcium levels, whereas the current-voltage relationship is linear at high calcium concentrations. This is normally explained by a calcium-binding site located in the electric field of the membrane, thereby facilitating calcium binding to the channel at positive voltages (Hartzell et al., 2005). This feature may be revealed by progressively lengthening the UV flash for photo-release of IP_3 to gradually increase the internal calcium level (Callamaras and Parker, 2000). As in other experiments, we found that voltage-clamp recording from control Axolotl oocytes revealed no IP_3-induced current even with a long UV flash (Figure 2A). In contrast, the xTMEM16A-induced current showed strong outward rectification with short UV flashes (Figures 2B, 2C, and 2E) but nearly linear current-voltage relationship with a long UV flash (Figures 2D and 2E), similar to the *Xenopus* oocyte CaCC current. By progressively increasing the duration of the UV flash and presumably the internal calcium rise (Callamaras and Parker, 2000), we found that a briefer UV flash, hence less calcium elevation, was required to cause half-maximal activation of the current at +40 mV than at −80 mV (Figures 2F and 2G), as expected if calcium binding to the channel is facilitated at positive voltages. Thus, the IP_3-induced current in Axolotl oocytes expressing xTMEM16A resembles the *Xenopus* oocyte CaCC current in the voltage dependence of calcium activation.

We then activated the channels generated by xTMEM16A using two other ways to elevate internal calcium, each time resulting in currents with outward rectification similar to the *Xenopus* oocyte CaCC. First, whereas control Axolotl oocytes showed no response to carbamylcholine (carbachol) (Figure 3A), carbachol induced currents in Axolotl oocytes injected with xTMEM16A cRNA (Figure 3B), likely because of endogenous

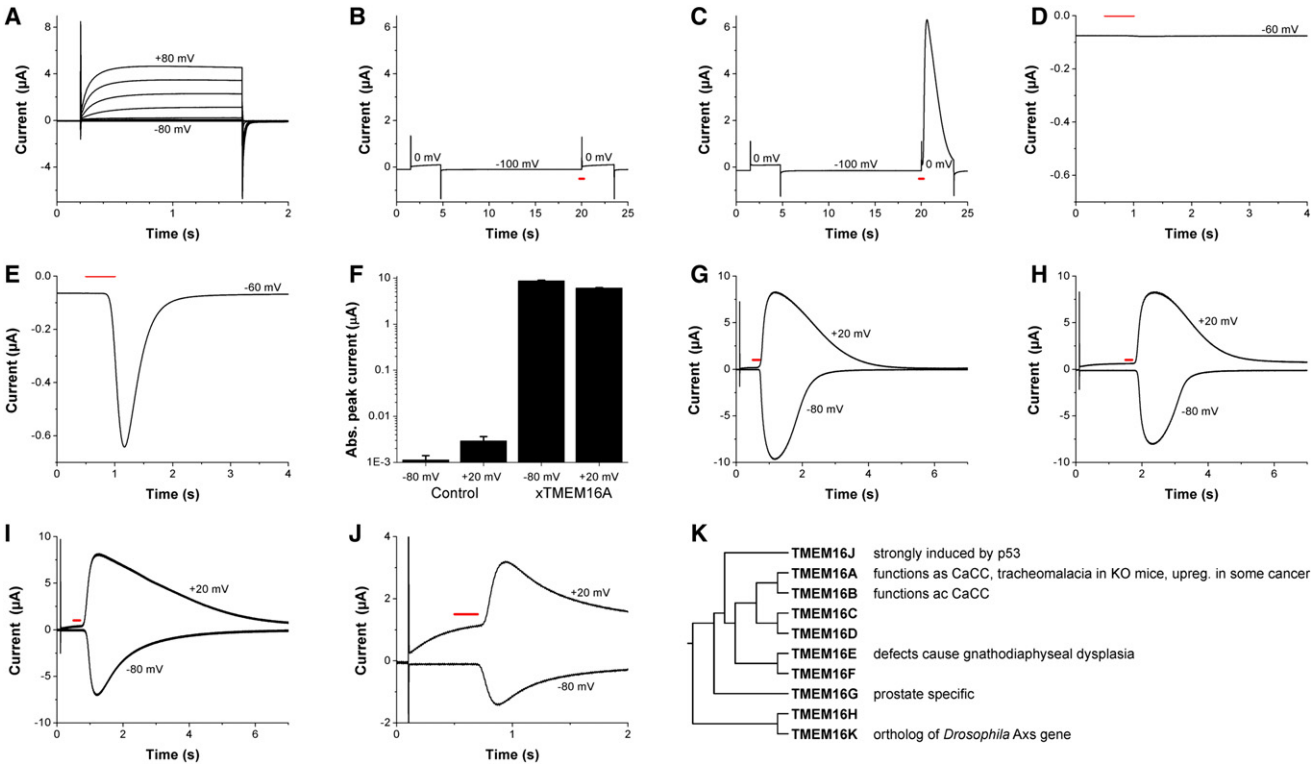

Figure 1. Expression Cloning of *Xenopus* Oocyte CaCC and Functional Expression of xTMEM16A and Its Mouse Homologs in Axolotl Oocytes

(A–J) Two-electrode voltage-clamp recording from Axolotl and *Xenopus* oocytes injected with various RNAs. With the exception of (A), all oocytes have been injected with caged IP_3 at least 1 hr before the experiment. The red bar indicates time of light flashes used for photo-release of IP_3.

(A) Uninjected Axolotl oocyte exhibiting endogenous voltage-gated proton currents. Oocyte was clamped to voltages between −80 mV and +80 mV in 20 mV steps. Holding potential was −60 mV.

(B and C) Axolotl oocyte expressing the SK2 Ca^{2+}-activated K^+ channels yielded current after Ca^{2+} increase because of flash photolysis but not after depolarization alone (C). No calcium-induced current was found in control oocytes injected with water (B). The holding potential was −100 mV.

(D and E) Unlike water-injected control oocytes (D), oocytes injected with *Xenopus* oocyte mRNA revealed new current after uncaging of IP_3. Holding potential was −60 mV.

(F) Peak amplitude of IP_3-induced currents at −80 mV and +20 mV in water-injected control oocytes and xTMEM16A cRNA-injected Axolotl oocytes (mean ± SEM, n = 10). The error bars represent the SEM.

(G) Endogenous Ca^{2+}-activated chloride currents from *Xenopus* oocyte measured at +20 mV and −80 mV after photo-release of IP_3. The holding potential was −60 mV.

(H–J) Ca^{2+}-activated currents similar to those in (G) are found in Axolotl oocytes injected with *Xenopus* TMEM16A cRNA (H), mouse TMEM16A (mTMEM16A-GFP) (I), and mouse TMEM16B (J). Note the difference in kinetics for outward and inward currents. The holding potential was −60 mV.

(K) Phylogenetic tree of human TMEM16 members generated with the MAFFT multiple sequence program (Katoh and Toh, 2008).

GPCR expression, and in oocytes coinjected with cRNAs for xTMEM16A and the m1 muscarinic acetylcholine receptor (m1AChR) (Figure 3C). These xTMEM16A-induced currents resemble the CaCC currents in *Xenopus* oocytes upon GPCR activation (Dascal, 1987; Takahashi et al., 1987).

Second, similar to the CaCC currents in *Xenopus* oocytes exposed first to the calcium ionophore A23187 and then to a high-calcium solution (Figure 3D), calcium-activated currents also appeared in Axolotl oocytes injected with xTMEM16A cRNA (Figure 3F) but not with water (Figure 3E). Voltage-clamp recordings of xTMEM16A-induced currents in A23187-treated Axolotl oocytes bathed in external solution at pH6.2 to close voltage-gated proton channels, which only open when the electrochemical gradient is outward (Decoursey, 2003), yielded very small currents in the absence of external calcium (Figure 3G) but large currents (Figure 3H) with outward rectification (Figure 3I) when external calcium concentration was raised. Carbachol-induced currents from Axolotl oocytes expressing xTMEM16A exhibited more pronounced outward rectification (Figure 3I), which correlates with their smaller amplitude as compared to currents in A23187-treated oocytes. This may be a reflection of the difference in internal calcium concentration, as in the case of Figure 2E. Thus, the xTMEM16A-induced current activated by elevation of internal calcium via calcium ionophore or GPCR stimulation exhibited outward rectification characteristic of the *Xenopus* oocyte CaCC.

Block of xTMEM16A-Induced Current by CaCC Blockers

To examine the pharmacological properties of xTMEM16A-induced current, we tested several CaCC blockers. We found DIDS (4,4′-diisothiocyanato-stilbene-2,2′-disulfonic acid) and

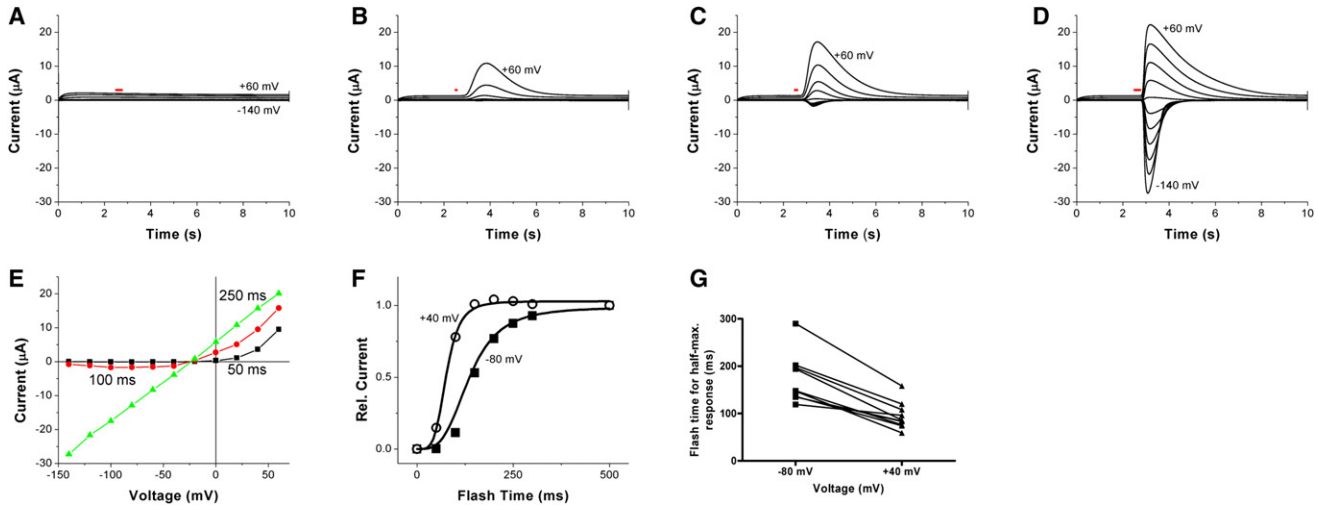

Figure 2. Calcium-Dependent Outward Rectification of IP_3-Induced Currents in Axolotl Oocytes Expressing *Xenopus* TMEM16A

(A) Two-electrode voltage-clamp recording from a water-injected Axolotl oocyte. Voltage steps range from −140 mV to +60 mV in 20 mV increments. The UV flash (indicated by red bar) lasted 250 ms. The holding potential was −60 mV.

(B–D) Axolotl oocyte injected with xTMEM16A cRNA (same voltage clamp as in [A]), with UV flash times of 50 ms (B), 100 ms (C), and 250 ms (D). The holding potential was −60 mV.

(E) IV curves of xTMEM16A-induced peak currents from the same oocytes ([B], black; [C], red; [D], green), showing that the outward rectification diminishes as UV flash is lengthened, causing increasing internal calcium concentration.

(F) Dependence of the xTMEM16A-induced outward and inward current amplitude on the duration of UV flash for photo-release of caged IP3. Current was normalized against the current induced by 500 ms UV flash (saturation condition). The correlation between UV flash duration and internal calcium level is not linear. For simplicity, we used the Hill curve for fitting data. UV flash durations necessary for half-maximal current at +40 mV and −80 mV were 76 ms and 106 ms, respectively. The error bars represent the SEM.

(G) Summary of recordings from several oocytes showing in each case the UV flash duration for half-maximal activation as determined from individual Hill plots is larger for the inward current at −80 mV (170 ± 16 ms) than for the outward current at +40 mV (95 ± 9 ms) (mean ± SEM). This voltage dependence is highly significant (Wilcoxon matched-pairs signed ranks test, $p < 0.002$). The error bars represent the SEM.

niflumic acid (NFA) to be more effective than NPPB [5-nitro-2-(3-phenylpropylalanine) benzoate] and DPC (diphenylamine-2-carboxyl acid) (Figure 3J). No significant block of xTMEM16A-induced current was found for tamoxifen at concentrations up to 100 μM (Figure 3J). The pharmacological profile of the xTMEM16A-induced current is in good agreement with that of the *Xenopus* oocyte CaCC (Hartzell et al., 2005).

Anion Selectivity of xTMEM16A-Induced CaCCs Resembles That of *Xenopus* Oocyte CaCCs

To verify that the calcium-activated channels generated by xTMEM16A are chloride channels, we showed that, like the *Xenopus* oocyte CaCC current, the xTMEM16A-induced current had a reversal potential that varied with external chloride concentration when chloride was replaced with the impermeant anion gluconate (53 ± 1 mV and 62 ± 3 mV per 10-fold concentration change, respectively) (Figure 4A). Moreover, the reversal potential was not altered by replacement of external sodium with calcium or N-methyl-D-glcamine (NMDG) (1 ± 3 mV and 3 ± 3 mV per 10-fold concentration change) (Figure 4A).

To test whether xTMEM16A gives rise to chloride channels with a preference for large anions as do *Xenopus* oocyte CaCCs (Qu and Hartzell, 2000), we replaced most of the external chloride (90 mM) with larger permeant anions. As we began with control experiments, we noticed that *Xenopus* oocytes in external thiocyanate (SCN^-) solution yielded CaCC current components with different anion selectivity: whereas the IP_3-induced CaCC currents were sustained for at least a couple of seconds in oocytes exposed to external thiocyanate, clamping the membrane potential at ∼−70 mV caused the faster current components to manifest as outward currents, whereas the slower current components appeared as inward currents (Figure 4B). Thus, these current components have different reversal potentials, some below and others above −70 mV. This phenomenon was also evident without voltage clamp: in *Xenopus* oocytes exposed to external bromide, iodide, or thiocyanate, IP_3-induced CaCC currents drove the membrane potential toward different levels at different times after the UV flash (Figure 4C). Whereas the membrane potential of *Xenopus* oocytes in isotonic chloride solution was driven toward the chloride equilibrium potential of around −20 mV upon CaCC activation, replacing 90 mM external chloride with thiocyanate revealed the presence of at least two CaCC current components with different permeability ratios, so that the membrane potential was first driven toward ∼−80 mV then toward ∼−70 mV regardless of whether the resting potential happened to be above (Figure 4C) or below (Figure 4D) −70 mV. These observations are in agreement with an earlier study suggesting that the multiple CaCC current components in *Xenopus* oocytes may have different anion selectivity (Kuruma and Hartzell, 1999). Previous studies have further raised the question of whether CaCC channels have multiple anion-binding sites with differential effects on channel gating (Perez-Cornejo

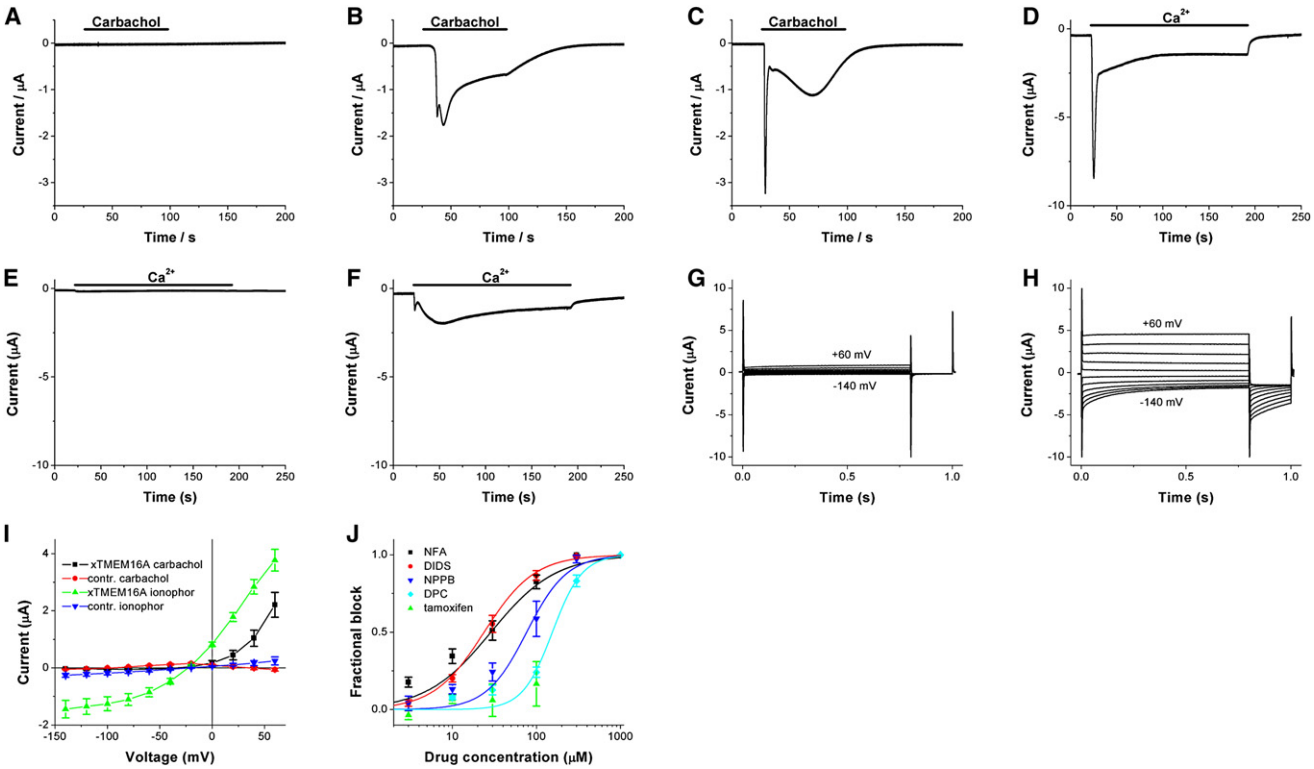

Figure 3. Carbachol- and Calcium-Induced Currents with Outward Rectification and Pharmacology of IP3-Induced Currents in Axolotl Oocytes Expressing *Xenopus* TMEM16A

(A–C) Two-electrode voltage-clamp traces of oocytes clamped at −60 mV and treated with 5 μM carbachol at time indicated.

(A) Typical current trace of a water-injected axolotl oocyte.

(B) Axolotl oocyte injected with xTMEM16A cRNA. The shape of carbachol-induced inward currents from different oocytes varies. In some oocytes, the fast component (first peak) was almost absent.

(C) Axolotl oocytes injected with xTMEM16A and human m1AChR cRNA. The current response of all tested oocytes showed a large early component and a more variable and smaller slow response (n = 10).

(D–F) Current response of A23187 pretreated oocytes to elevation of external calcium from 0 to 5 mM at the time indicated by the horizontal bar. Oocytes were clamped at −60 mV.

(D) Recording from uninjected *Xenopus* oocyte showing the two typical CaCC components. The slow component is more variable.

(E) Typical trace from an uninjected Axolotl oocyte.

(F) Recording from an Axolotl oocyte injected with xTMEM16A cRNA. Fast and slow components showed variability.

(G and H) Voltage-clamp recording from an A23187-treated Axolotl oocyte injected with xTMEM16A cRNA at pH6.2 in Ca^{2+}-free solution (G) and 90 s after elevating external calcium to 5 mM (H). Oocytes were clamped from −30 mV to voltages between −140 and +60 mV in 20 mV steps.

(I) Voltage dependence of current amplitude induced by carbachol application for 90 s, or Ca^{2+} elevation subsequent to A23187 exposure in xTMEM16a cRNA or water-injected oocytes. Amplitude in the IV curve (mean ± SEM, n = 10 each) was measured at 0.75 s after the voltage step from a holding potential at −30 mV to the indicated potential. The error bars represent the SEM.

(J) Dose-response curves for the xTMEM16A-induced current block by different CaCC blockers determined by measurement of IP_3-induced peak current at +20 mV. The holding potential was −30 mV. For each oocyte, the current block as function of blocker concentration was fitted with a Hill curve to yield the dissociation constant (K) and Hill coefficient (N). Curves shown are based on the means of those values determined from individual fits. Values given below are mean ± SEM. NFA (black squares): K = 29 ± 6 μM, N = 1.1 ± 0.1 (n = 10). DIDS (red circles): K = 24 ± 2 μM, N = 1.4 ± 0.2 (n = 6). NPPB (blue triangle): K = 77 ± 21 μM, N = 1.8 ± 0.3 (n = 6). DPC (turquoise diamond): K = 155 ± 13 μM, N = 2.5 ± 0.4 (n = 6). Tamoxifen (green triangle): no dissociation constant or Hill coefficient could be determined because of limited solubility (n = 8). The error bars represent the SEM.

et al., 2004) and whether the complex time course of the *Xenopus* oocyte CaCC current is attributable to multiple channel types or one CaCC with multiple open states (Boton et al., 1989; Lupu-Meiri et al., 1989). Because some ion channels exhibit time-dependent changes in ion selectivity (Khakh and Lester, 1999), we wondered whether the xTMEM16A-induced CaCC might have multiple open states with different ion selectivity.

Indeed, Axolotl oocytes expressing xTMEM16A yielded multiple current components with different reversal potentials: in an Axolotl oocyte with more depolarized membrane potential, exposure to external iodide or thiocyanate caused the IP_3-induced CaCC activity to drive the membrane potential first below and then above the resting potential (Figure 4F). In oocytes with more hyperpolarized membrane potential, under bi-ionic conditions, the CaCC activation also caused the membrane potential to be driven first quickly toward one reversal potential and then slowly toward another, more depolarized, reversal potential (Figure 4E). These studies show that xTMEM16A-induced CaCCs

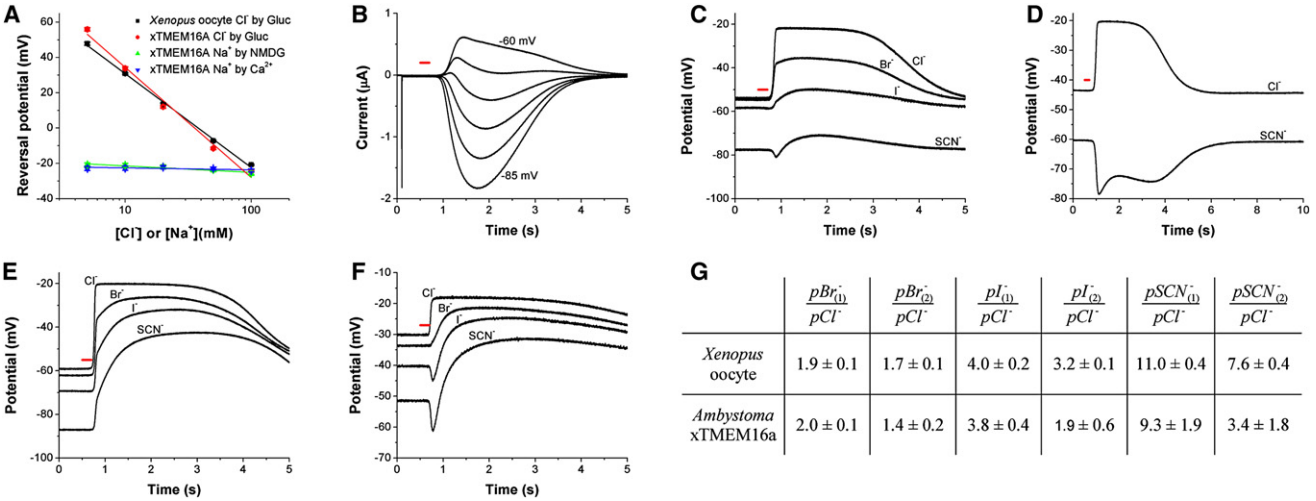

G

	$\frac{pBr^-_{(1)}}{pCl^-}$	$\frac{pBr^-_{(2)}}{pCl^-}$	$\frac{pI^-_{(1)}}{pCl^-}$	$\frac{pI^-_{(2)}}{pCl^-}$	$\frac{pSCN^-_{(1)}}{pCl^-}$	$\frac{pSCN^-_{(2)}}{pCl^-}$
Xenopus oocyte	1.9 ± 0.1	1.7 ± 0.1	4.0 ± 0.2	3.2 ± 0.1	11.0 ± 0.4	7.6 ± 0.4
Ambystoma xTMEM16a	2.0 ± 0.1	1.4 ± 0.2	3.8 ± 0.4	1.9 ± 0.6	9.3 ± 1.9	3.4 ± 1.8

Figure 4. *Xenopus* Oocyte CaCC and xTMEM16A-Induced CaCC Have Multiple Current Components with Different Anion Selectivity

(A) Reversal potential of IP_3-induced conductance as function of the extracellular Cl^- concentration (Cl^- has been substituted with gluconate). In *Xenopus* oocytes (red circles, n = 10) and Axolotl oocytes injected with xTMEM16A cRNA (black squares, n = 8), the slopes (53 ± 1 mV and 62 ± 3 mV per 10-fold concentration change) are typical of Cl^- channels. Replacing external sodium with calcium ($2Na^+$ by $1Ca^{2+}$ + 1glucose, blue triangle) or NMDG (green triangle) had no significant effect on the reversal potential (1 ± 3 mV and 3 ± 3 mV per 10-fold concentration change). The error bars represent the SEM.

(B) Voltage-clamp traces of *Xenopus* oocyte in high-SCN^- solution clamped in 5 mV steps from −85 mV to −60 mV. Whereas the CaCC currents were sustained for at least a couple of seconds after the UV flash, clamping of the membrane potential at −70 mV caused some of the current components to manifest as outward currents, whereas others appeared as inward currents. The red bar indicates time of light flashes used for photo-release of IP_3.

(C–F) Membrane potential traces from oocytes perfused with high-Cl^-, high-Br^-, high-I^-, and high-SCN^- solutions (see the Experimental Procedures). Recordings were made with a single electrode. After photo-release of IP_3 (red bar), the Ca^{2+}-activated chloride channels dominate the cellular conductance, and the membrane potential can be used as estimation of the reversal potential of CaCCs.

(C and D) Traces from *Xenopus* oocyte. In *Xenopus* oocytes exposed to external bromide, iodide or thiocyanate, IP_3-induced CaCC currents drove the membrane potential toward different levels at different times (C). Whereas *Xenopus* oocytes in isotonic chloride solution were driven toward the chloride equilibrium potential of around −20 mV upon CaCC activation, replacement of 90 mM external chloride with thiocyanate revealed the presence of at least two CaCC current components with different permeability ratio, so that the membrane potential was first driven toward ∼−80 mV (C) then toward ∼−70 mV regardless of whether the resting potential happened to be above (D) or below (C) −70 mV. The oocyte used in (C) is the same as that in (B).

(E and F) Traces from axolotl oocytes injected with xTMEM16A cRNA. In an Axolotl oocyte with more depolarized membrane potential, exposure to external iodide or thiocyanate caused the IP_3-induced CaCC activity to drive the membrane potential first below and then above the resting potential (F). In oocytes with more hyperpolarized membrane potential, under bi-ionic conditions the CaCC activation caused the membrane potential to be driven first quickly toward one reversal potential and then slowly toward another, more depolarized, reversal potential (E). Although traces shown in (C) and (E) are more typical, a fast and at least one slow component with different reversal potential in bi-ionic conditions are more obvious in (D) and (F).

(G) Permeability ratios (mean ± SEM) calculated from changes of reversal potentials for different anions. The index 1 refers to the permeability ratio immediately after Ca^{2+} increase and channel opening. In a simple model, the majority of the open channels might be in the same fast state. For the calculation of permeability ratios with index 2, the most positive reversal potential determined under bi-ionic conditions was used. At this point, ion channels might occupy various slower states, and differences in permeability ratios between *Xenopus* oocytes and Axolotl oocytes injected with xTMEM16A cRNA are likely due to differences in the occupation of these states.

exhibit greater permeability for larger anions than for chloride, as do CaCCs in many cell types (Hartzell et al., 2005). Moreover, they give rise to multiple CaCC current components displaying different anion selectivity as do *Xenopus* oocyte CaCCs, though they all have the same permeability series of $pSCN^- > pI^- > pBr^- > pCl^-$ (Figure 4G). Notably, the permeability ratios for the first (faster) current component are in good agreement with those reported for CaCCs in *Xenopus* oocytes and other cell types as determined by patch-clamp recordings in steady-state conditions (Qu and Hartzell, 2000). The expression cloning of xTMEM16A has therefore revealed that the calcium-activated chloride channel it produces likely has multiple open states that differ not only in kinetics but also in anion selectivity. It will be interesting to determine in future studies whether these open states correspond to the *Xenopus* oocyte CaCC current components with different kinetics and calcium sensitivity (Boton et al., 1989).

Functional Expression of mTMEM16A in Mammalian HEK293 Cells

If TMEM16A encodes a CaCC, its functional expression in multiple expression systems should be possible. Indeed, not only did mTMEM16A-GFP generate CaCCs in Axolotl oocytes (Figure 1I), but transfection of human embryonic kidney HEK293 cells with mTMEM16A-GFP also yielded large CaCC current if the pipette solution contained 500 nM calcium (Figures 5A and 5D), whereas no new current appeared if the pipette solution contained no free calcium (Figures 5C and 5D). Control HEK293 cells transfected with GFP did not give rise to substantial currents even with 500 nM calcium in the pipette solution (Figures 5B and 5D). Besides a moderate voltage dependence of the deactivation time constant (Figure 5F), the mTMEM16A-induced CaCC current exhibited outward rectification (Figure 5E), similar to a recent report of mTMEM16A functional expression in HEK293 cells (Yang

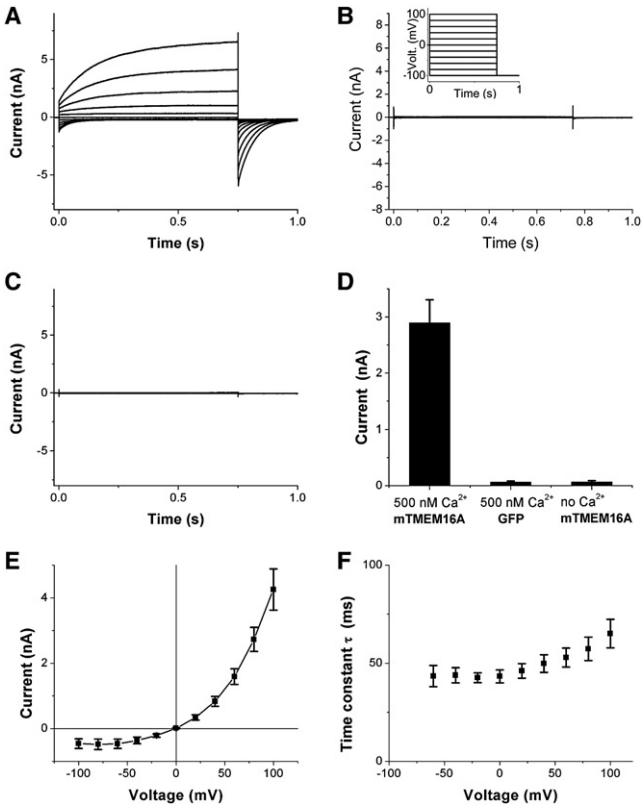

Figure 5. Ca^{2+}-Activated Currents in HEK293 Cells Expressing mTMEM16A-GFP

(A) Representative whole-cell recording from a HEK293 cell transfected with mTMEM16A-GFP. The patch pipette contained 500 nM free calcium. The cell was clamped from the holding potential (0 mV) to voltages between −100 and +100 mV in 20 mV steps followed by a step to −100 mV (see [B], inset). The same protocol (see the Experimental Procedures) was used in (B) and (C).

(B) Whole-cell recording from a HEK293 cell transfected with GFP. The patch pipette contained 500 nM free calcium.

(C) Whole-cell recording from a HEK293 cell transfected with mTMEM16A-GFP. The patch pipette contained 0 nM free calcium.

(D) Bar graph showing the mean and SEM of whole-cell currents measured 0.75 s after depolarization to +80 mV (n = 10 each). All recordings were performed 3 to 5 min after break in. The typical TMEM16A current was observed in all ten TMEM16A-GFP-transfected cells under 500 nM Ca^{2+} but not in GFP-transfected cells. Three of the TMEM16A-GFP-transfected cells showed significant currents immediately after break in with Ca^{2+} free pipette solution, but these currents disappeared within 3 min. Possible explanations include slow diffusion of calcium buffer, calcium leakage during break in, and slow channel closure conceivably involving calcium-depending enzymes.

(E) IV curve (mean and SEM) showing outward rectification for the same set of experiments.

(F) Time constant of deactivation (mean and SEM, n = 10) of Ca^{2+}-activated currents as function of membrane potential, from whole-cell patch-clamp recording of HEK293 cells expressing mTMEM16A-GFP.

The error bars in (D)–(F) represent the SEM.

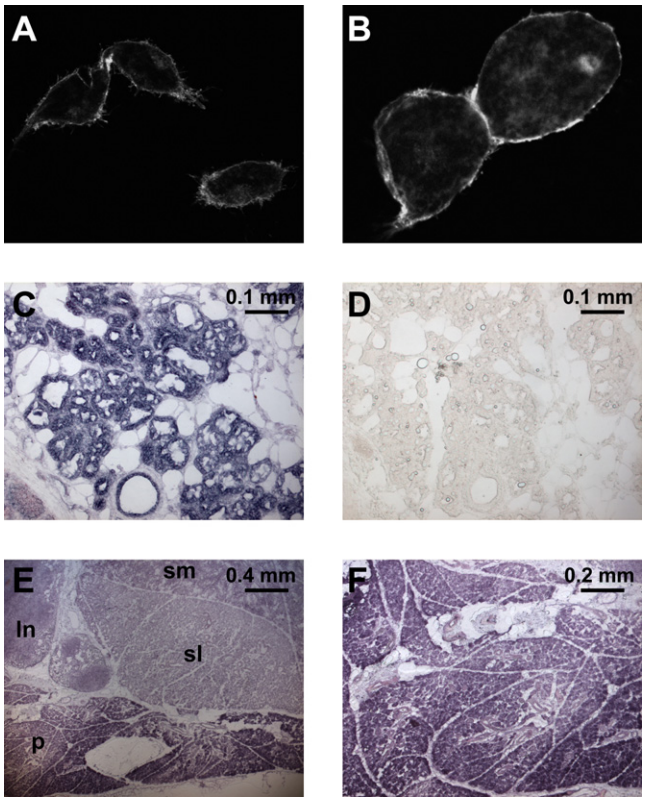

Figure 6. Surface Expression of TMEM16A-GFP and TMEM16A mRNA Expression in Mammary and Salivary Glands

(A and B) Confocal image of HEK293 cells transfected with mTMEM16A-GFP. A strong GFP signal is visible in the plasma membrane. We noticed that cells expressing mTMEM16A detach more easily from the surface and have a rounder appearance than do GFP transfected cells.

(C and D) In situ hybridization of mouse mammary gland (day 18 of pregnancy) with antisense probe (C) directed against mTMEM16A. A strong signal is visible in epithelial cells of the alveoli. No signal appears in control with an mTMEM16A sense probe (D).

(E) In situ hybridization of mouse salivary glands. TMEM16A expression is high in all epithelial cells but highest in acinar cells of parotid gland. ln, lymph node; p, parotid gland; sl, sublingual gland; sm, submandibular gland.

(F) In situ hybridization of mouse parotid gland with an mTMEM16A antisense probe.

et al., 2008). Thus, mTMEM16A as well as xTMEM16A generated CaCCs with outward rectification characteristic of native CaCCs (Callamaras and Parker, 2000; Evans and Marty, 1986; Kuruma and Hartzell, 1999).

Surface Expression and Broad Tissue Distribution of TMEM16A

As expected for a CaCC channel protein, the GFP-tagged TMEM16A displayed prominent surface expression (Figures 6A and 6B), in agreement with the reported surface expression of TMEM16A (Rock et al., 2008; West et al., 2004; Yang et al., 2008) and other family members, including TMEM16E (Mizuta et al., 2007), TMEM16G (Bera et al., 2004), and the yeast Ist2 (Juschke et al., 2005; Takizawa et al., 2000).

The hTMEM16A mRNA is present in multiple human tissues, including liver, skeletal muscle, heart, lung, placenta, and small intestine (Huang et al., 2006). The mTMEM16A mRNA is expressed in foregut and airway epithelia as well as tracheal smooth muscle (Rock et al., 2008), and the mTMEM16A protein has been found in epithelial cells in the lung and kidney, acinar

cells in the pancreas and submandibular gland, and sensory neurons (Yang et al., 2008). The NCBI UniGene EST analyses of human and mouse TMEM16A further show expression in several glands, plus the eye, tongue, and kidney, in addition to those tissues included in the northern analysis (Huang et al., 2006). As CaCCs have been implicated in mammary epithelial fluid transport regulation by purine nucleotides (Blaug et al., 2003), we further confirmed mTMEM16A mRNA expression in mammary glands (Figure 6C); no in situ hybridization signals were detectable with control sense probes (Figure 6D). There was also high expression of mTMEM16A mRNA in salivary glands (Figure 6E), including parotid glands (shown at higher magnification in Figure 6F), which respond to parasympathetic stimulation of muscarinic acetylcholine receptors with a rise of intracellular IP_3 and calcium, thereby activating CaCCs to drive fluid secretion (Melvin et al., 2005). The expression patterns of mammalian TMEM16A, taken together with the functional properties of CaCCs generated by xTMEM16A or mTMEM16A, provide strong support for the correspondence between TMEM16A and CaCC.

DISCUSSION

In this study, we report expression cloning of calcium-activated chloride channels endogenous to *Xenopus* oocytes, yielding a member of the evolutionarily conserved TMEM16 family that includes TMEM16E (GDD1) linked to the human disease *gnathodiaphyseal dysplasia* (Tsutsumi et al., 2004). Taken together with the ability of both mTMEM16A and mTMEM16B to generate CaCCs in Axolotl oocytes and the predominant surface distribution of mTMEM16A proteins associated with CaCC expression in HEK293 cells, the close resemblance of xTMEM16A-induced CaCC to the endogenous *Xenopus* oocyte CaCC supports the notion that TMEM16A is a calcium-activated chloride channel subunit. This notion is consistent with the phenotype of increased sodium tolerance in yeast lacking Ist2 (Entian et al., 1999). Moreover, mice lacking mTMEM16A fail to thrive and die with aerophagia and little weight gain within 10 days after birth (Rock et al., 2008), implicating an essential function of TMEM16A expressed in the airway and foregut epithelia. Future genetic, biophysical, and biochemical studies may determine the composition and physiological functions of CaCCs that contain TMEM16A or its family members in different organisms, including animals, fungi, and plants.

Remarkably, the TMEM16A-induced calcium-activated chloride channel likely has multiple open states that differ not only in kinetics but also in anion selectivity. Whereas the test for pore-lining channel subunits has traditionally been a demonstration of mutations that alter ion selectivity, this criterion cannot be used here since altered selectivity could also result from mutations that affect gating transitions between CaCC open states with different anion selectivity. For this reason, we regard TMEM16A for the moment simply as a CaCC subunit. Given that the *Xenopus* oocyte CaCC has a small single-channel conductance of ~3 pS (Takahashi et al., 1987), the large xTMEM16A-induced CaCC currents must correspond to the surface expression of millions of CaCC channels. Considering the robust TMEM16A-induced CaCC expression accompanied with prominent TMEM16A surface expression within 1 day of cRNA injection into Axolotl oocytes or transfection of HEK293 cells, it will be of interest to determine whether CaCC channels traffic from endoplasmic reticulum to the plasma membrane via a novel mechanism, as reported for the yeast TMEM16 homolog (Juschke et al., 2005).

In summary, we have identified TMEM16A as a gene encoding the calcium-activated chloride channel exhibiting the CaCC hallmark features of calcium and voltage dependence, anion selectivity, and broad expression patterns. Whereas this study focuses primarily on the *Xenopus* oocyte CaCC, the strong evolutionary conservation of the TMEM16 family from paramecium and fungi to plants and animals will likely facilitate studies of CaCCs in various tissue types of diverse organisms, including the yeast Ist2 (Increased sodium tolerance) confined to the daughter cell membrane because of targeted transport of its transcript to the bud tip (Takizawa et al., 2000). It is worth keeping in mind that whereas some TMEM16 family members give rise to CaCCs on the cell membrane, other family members may have functions in intracellular membrane compartments, as exemplified by the *Drosophila* Axs (Aberrant X segregation) protein that resides in a membranous structure that surrounds the meiotic spindle (Kramer and Hawley, 2003). It is also noteworthy that the human TMEM16A gene is amplified or overexpressed in multiple cancers associated with poor prognosis (Carles et al., 2006; Huang et al., 2006; West et al., 2004), raising the question whether CaCC modulators may be considered for cancer treatment. The ability of mTMEM16A to produce CaCC in multiple expression systems will hopefully enable the development of specific CaCC modulators valuable for both physiological studies and therapeutic purposes. Because the mild airway phenotype in mice without CFTR appears to correlate with the presence of the "alternative" plasma membrane chloride conductance, namely CaCC (Clarke et al., 1994), one strategy for bypassing the chloride secretory defect in cystic fibrosis is to activate CaCCs on the airway apical membrane (Anderson et al., 1992; Boucher et al., 1989; Clarke et al., 1994; Tarran et al., 2006). Modulators of CaCCs that control the volume of the airway surface liquid bathing the airway epithelial cilia, whose proper movement is crucial for mucus clearing, may also be considered for treating chronic obstructive pulmonary diseases like bronchitis and asthma (Tarran et al., 2006; Widdicombe, 2002). Moreover, blockers specific for CaCCs could be beneficial for treating hypertension, given the role of CaCCs in sustaining membrane depolarization, calcium rise, and vascular tone (Large and Wang, 1996).

EXPERIMENTAL PROCEDURES

RNA Isolation

RNA was isolated from *Xenopus laevis* ovary with the RNeasy Maxi Kit (QIAGEN) and then run through Oligo-dT cellulose columns (Molecular Research Center) twice. For size fractionation, 150–200 μg of the heat-denatured poly(A)$^+$ RNA was separated on a nondenaturing 0.8% Tris-acetate-ethylenediamine tetraacetic acid (TAE) agarose gel at 3 V/cm for 3 hr, electroeluted at 100 V for 12 hr with the Elutrap system (Schleicher & Shuell), precipitated with isopropanol, and dissolved in water.

Library Construction

cDNA synthesis followed the Gubler-Hoffman method (Gubler and Hoffman, 1983) and the reverse transcriptase manufacturer's instructions, with some modifications. First strands of cDNAs were synthesized from

non-size-fractionated poly(A)$^+$ RNA with Superscript III (Stratagene) and a I-CeuI-oligo(dT) primer/adaptor for 60 min at 50°C. After second-strand synthesis, cDNAs were blunted with T4 polymerase, phosphorylated, cut with I-CeuI (New England Biolabs), and size fractionated on a 0.7% low-melting-point agarose gel (SeaPlaque GTG agarose, Lonza). Fragments larger than 5 kb were purified and ligated to HpaI/CeuI cut arms of the oocyte expression vector pBaer6 (B.C.S., unpublished data), a derivative of the N15 prophage-based linear plasmid pG591 (Ravin et al., 2003) in which the multiple cloning site is flanked by 3′ and 5′ beta globin sequences, with the latter preceded by a T7 promoter to allow RNA synthesis. *Escherichia coli* were transformed and plated on ten master plates at a density of ~5000 clones/plate. For each pool, cRNA was transcribed from I-CeuI digested DNA with T7 polymerase, injected into Axolotl oocytes, and assayed for the presence of Ca^{2+} activated Cl^- currents (see below). A positive pool was identified and subsequently subdivided until a single clone was obtained.

cDNA Cloning

Expressed sequence tags (IMAGE Consortium cDNA clones [Lennon et al., 1996], numbers 30547439 and 5357763) homologous to TMEM16A from mouse (mTMEM16A), mTMEM16B, and the full-length clone for *Xenopus* TMEM16A were subcloned into pGEM via standard molecular biological techniques. For expression in mammalian cells, mouse TMEM16A was subcloned in frame into pEGFP-N1 vector, resulting in a plasmid coding for a C-terminal GFP-tagged mTMEM16A fusion protein.

Oocyte Electrophysiology

For experiments involving TMEM16 constructs, capped cRNA was in vitro transcribed from linearized plasmids with the mMessage mMachine kit (Ambion). Female Axolotls and *Xenopus laevis* were purchased from the *Ambystoma* Genetic Stock Center and Nasco, respectively. Oocytes from these animals were defoliculated by treatment with collagenase. Usually 0.5–5 ng of cRNA (50 ng for mRNA) was injected into defolliculated oocytes. Oocytes were kept at 17°C in ND96 solution (96 mM NaCl, 2 mM KCl, 1.8 mM $CaCl_2$, 1 mM $MgCl_2$, 10 mM HEPES [pH 7.4]). Two-electrode voltage-clamp measurements were performed at room temperature 2–4 days after injection with a GeneClamp500 amplifier (Axon Instruments) and pClamp 8.0 software (Axon Instruments). Oocytes used in photolysis experiments were injected with 50 μl of 100 μM caged inositol trisphosphate [*myo*-inositol 1,4,5-trisphosphate, *P*4(5)-1-(2-nitrophenyl) ethyl ester] (Molecular Probes) at least 1 hr before recording and kept in the dark until usage. For flash photolysis, light derived from a mercury arc lamp was guided by a fused silica fiber (Oriel) to the top of oocytes in the recording chamber. Flash time was controlled via electronic shutter. For screening primary pools of the *Xenopus* library, we used *Ambystoma mexicanum* oocytes at stage IV and V. After loading with caged inositol trisphosphate, such oocytes showed in our setup consistently less than 10 nA Ca^{2+} activated current when held at −80 mV and illuminated with a UV flash for 200 ms. As the pool size was gradually reduced, we could also use stage VI Axolotl oocytes with slightly larger endogenous Ca^{2+} activated currents, which are generally less than 30 nA.

Currents were usually recorded in Ca^{2+}-free ND96 solution (96 mM NaCl, 2 mM KCl, 3 mM $MgCl_2$, 10 mM HEPES [pH 7.4]). Solutions for experiments involving Cl^- replacement with gluconate were prepared from appropriate mixtures of solutions containing high Cl^- (95 mM NaCl, 1 mM KCl, 2 mM $MgCl_2$, 10 mM HEPES [pH 7.4]) and solutions containing high gluconate (95 mM NaGluconate, 1 mM KCl, 2 mM $MgCl_2$, 10 mM HEPES [pH 7.4]). In other permeability experiments, solutions containing 90 mM NaX, 2 mM KCl, 4 mM MgCl, and 10 mM HEPES (pH 7.4) with X = Cl^-, Br^-, I^-, or SCN^- were used. The permeability ratios were calculated from shifts in reversal potential ΔErev with the Goldman-Hodgkin-Katz Equation. For data analysis, we used Clampfit8 (Axon Instruments) and Origin 7.0 (OriginLab).

Patch-Clamp Recordings

HEK293 cells were seeded on glass coverslips coated with PureCol (Inamed) and transfected with mouse TMEM16A-EGFP or EGFP expression plasmids (both in pEGFP-N1 vector) with FuGENE 6 (Roche). Whole-cell recordings were performed at room temperature on cells showing weak EGFP fluorescence within 3 days after transfection with an Axopatch 200B patch-clamp amplifier and pClamp9 software (Molecular Devices). The extracellular solution contained 140 mM NMDG-Cl, 5 mM KCl, 2 mM $CaCl_2$, 1 mM $MgCl_2$, and 10 mM NMDG-HEPES. Zero calcium pipette solution contained 140 mM NMDG-Cl, 10 mM EDTA, and 10 mM NMDG-HEPES. Five hundred nanomolar free Ca^{2+} pipette solution was prepared with the pH-metric method (Tsien and Pozzan, 1989) and contained 140 mM NMDG-Cl, 7.4 mM Ca^{2+}-EGTA, 2.6 mM NMDG-EGTA, and 10 mM NMDG-HEPES. pH of all solutions was 7.2, titrated with N-methyl-D-glucamine (NMDG). Calculation of free Ca^{2+} concentration was done with WEBMAXC software (http://www.stanford.edu/~cpatton/maxc.html).

Protein Localization

Transfected HEK293 cells were fixed with 4% paraformaldehyde and 0.4% sucrose in phosphate-buffered saline (PBS) for 15 min, washed with PBS, and mounted onto slides for image acquisition with a Zeiss LSM 510 confocal microscope.

In Situ Hybridization

Mouse TMEM16A antisense and sense cRNA probes were synthesized with the DIG labeling system (Roche Biosciences) according to the manufacturer's instructions. In situ hybridization was carried out according to Schaeren-Wiemers and Gerfin-Moser (1993).

ACCESSION NUMBERS

The cDNA sequence reported in this paper has been deposited in the GenBank database with the accession number EU367938.

ACKNOWLEDGMENTS

We thank J. Adelman for SK2 cDNA and N.V. Ravin for the pG591 clone. We are grateful for the help of C. Han with confocal images, T. Müller with image acquisition, X. Qian with patch-clamp experiments, and D. Wang with in situ hybridizations. We also thank P. Lu and P. Soba for discussion. This work was supported by a Human Frontier Science Program fellowship to B.C.S. and a National Institute of Mental Health grant to L.Y.J. L.Y.J. and Y.N.J. are Howard Hughes Medical Institute investigators.

Received: July 30, 2008
Revised: September 3, 2008
Accepted: September 3, 2008
Published: September 18, 2008

REFERENCES

Anderson, M.P., Sheppard, D.N., Berger, H.A., and Welsh, M.J. (1992). Chloride channels in the apical membrane of normal and cystic fibrosis airway and intestinal epithelia. Am. J. Physiol. *263*, L1–L14.

Arreola, J., Melvin, J.E., and Begenisich, T. (1995). Inhibition of Ca(2+)-dependent Cl- channels from secretory epithelial cells by low internal pH. J. Membr. Biol. *147*, 95–104.

Bader, C.R., Bertrand, D., and Schwartz, E.A. (1982). Voltage-activated and calcium-activated currents studied in solitary rod inner segments from the salamander retina. J. Physiol. *331*, 253–284.

Barish, M.E. (1983). A transient calcium-dependent chloride current in the immature Xenopus oocyte. J. Physiol. *342*, 309–325.

Barish, M.E., and Baud, C. (1984). A voltage-gated hydrogen ion current in the oocyte membrane of the axolotl, Ambystoma. J. Physiol. *352*, 243–263.

Barro-Soria, R., Schreiber, R., and Kunzelmann, K. (2008). Bestrophin 1 and 2 are components of the Ca(2+) activated Cl(-) conductance in mouse airways. Biochim. Biophys. Acta, in press. Published online July 3, 2008.

Bera, T.K., Das, S., Maeda, H., Beers, R., Wolfgang, C.D., Kumar, V., Hahn, Y., Lee, B., and Pastan, I. (2004). NGEP, a gene encoding a membrane protein detected only in prostate cancer and normal prostate. Proc. Natl. Acad. Sci. USA *101*, 3059–3064.

Blaug, S., Rymer, J., Jalickee, S., and Miller, S.S. (2003). P2 purinoceptors regulate calcium-activated chloride and fluid transport in 31EG4 mammary epithelia. Am. J. Physiol. Cell Physiol. *284*, C897–C909.

Boton, R., Dascal, N., Gillo, B., and Lass, Y. (1989). Two calcium-activated chloride conductances in Xenopus laevis oocytes permeabilized with the ionophore A23187. J. Physiol. *408*, 511–534.

Boucher, R.C., Cheng, E.H., Paradiso, A.M., Stutts, M.J., Knowles, M.R., and Earp, H.S. (1989). Chloride secretory response of cystic fibrosis human airway epithelia. Preservation of calcium but not protein kinase C- and A-dependent mechanisms. J. Clin. Invest. *84*, 1424–1431.

Callamaras, N., and Parker, I. (2000). Ca(2+)-dependent activation of Cl(-) currents in Xenopus oocytes is modulated by voltage. Am. J. Physiol. Cell Physiol. *278*, C667–C675.

Carles, A., Millon, R., Cromer, A., Ganguli, G., Lemaire, F., Young, J., Wasylyk, C., Muller, D., Schultz, I., Rabouel, Y., et al. (2006). Head and neck squamous cell carcinoma transcriptome analysis by comprehensive validated differential display. Oncogene *25*, 1821–1831.

Clarke, L.L., Grubb, B.R., Yankaskas, J.R., Cotton, C.U., McKenzie, A., and Boucher, R.C. (1994). Relationship of a non-cystic fibrosis transmembrane conductance regulator-mediated chloride conductance to organ-level disease in Cftr(−/−) mice. Proc. Natl. Acad. Sci. USA *91*, 479–483.

Dascal, N. (1987). The use of Xenopus oocytes for the study of ion channels. CRC Crit. Rev. Biochem. *22*, 317–387.

Decoursey, T.E. (2003). Voltage-gated proton channels and other proton transfer pathways. Physiol. Rev. *83*, 475–579.

Eggermont, J. (2004). Calcium-activated chloride channels: (un)known, (un)loved? Proc. Am. Thorac. Soc. *1*, 22–27.

Entian, K.D., Schuster, T., Hegemann, J.H., Becher, D., Feldmann, H., Guldener, U., Gotz, R., Hansen, M., Hollenberg, C.P., Jansen, G., et al. (1999). Functional analysis of 150 deletion mutants in Saccharomyces cerevisiae by a systematic approach. Mol. Gen. Genet. *262*, 683–702.

Evans, M.G., and Marty, A. (1986). Calcium-dependent chloride currents in isolated cells from rat lacrimal glands. J. Physiol. *378*, 437–460.

Frings, S., Reuter, D., and Kleene, S.J. (2000). Neuronal Ca2+ -activated Cl- channels–homing in on an elusive channel species. Prog. Neurobiol. *60*, 247–289.

Fromm, J., and Lautner, S. (2007). Electrical signals and their physiological significance in plants. Plant Cell Environ. *30*, 249–257.

Gubler, U., and Hoffman, B.J. (1983). A simple and very efficient method for generating cDNA libraries. Gene *25*, 263–269.

Hartzell, C., Putzier, I., and Arreola, J. (2005). Calcium-activated chloride channels. Annu. Rev. Physiol. *67*, 719–758.

Huang, X., Godfrey, T.E., Gooding, W.E., McCarty, K.S., Jr., and Gollin, S.M. (2006). Comprehensive genome and transcriptome analysis of the 11q13 amplicon in human oral cancer and synteny to the 7F5 amplicon in murine oral carcinoma. Genes Chromosomes Cancer *45*, 1058–1069.

Jego, P., Lerivray, H., Chesnel, A., and Charbonneau, M. (1986). Urodele egg jelly and fertilization. Adv. Exp. Med. Biol. *207*, 205–233.

Juschke, C., Wachter, A., Schwappach, B., and Seedorf, M. (2005). SEC18/NSF-independent, protein-sorting pathway from the yeast cortical ER to the plasma membrane. J. Cell Biol. *169*, 613–622.

Katoh, K., and Toh, H. (2008). Recent developments in the MAFFT multiple sequence alignment program. Brief. Bioinform. *9*, 286–298.

Khakh, B.S., and Lester, H.A. (1999). Dynamic selectivity filters in ion channels. Neuron *23*, 653–658.

Kramer, J., and Hawley, R.S. (2003). The spindle-associated transmembrane protein Axs identifies a membranous structure ensheathing the meiotic spindle. Nat. Cell Biol. *5*, 261–263.

Kuruma, A., and Hartzell, H.C. (1999). Dynamics of calcium regulation of chloride currents in Xenopus oocytes. Am. J. Physiol. *276*, C161–C175.

Large, W.A., and Wang, Q. (1996). Characteristics and physiological role of the Ca(2+)-activated Cl- conductance in smooth muscle. Am. J. Physiol. *271*, C435–C454.

Lennon, G., Auffray, C., Polymeropoulos, M., and Soares, M.B. (1996). The I.M.A.G.E. Consortium: An integrated molecular analysis of genomes and their expression. Genomics *33*, 151–152.

Lupu-Meiri, M., Shapira, H., and Oron, Y. (1989). Dual regulation by protein kinase C of the muscarinic response in Xenopus oocytes. Pflugers Arch. *413*, 498–504.

Melvin, J.E., Yule, D., Shuttleworth, T., and Begenisich, T. (2005). Regulation of fluid and electrolyte secretion in salivary gland acinar cells. Annu. Rev. Physiol. *67*, 445–469.

Miledi, R. (1982). A calcium-dependent transient outward current in Xenopus laevis oocytes. Proceedings of the Royal Society of London. Series B, *215*, 491–497.

Mizuta, K., Tsutsumi, S., Inoue, H., Sakamoto, Y., Miyatake, K., Miyawaki, K., Noji, S., Kamata, N., and Itakura, M. (2007). Molecular characterization of GDD1/TMEM16E, the gene product responsible for autosomal dominant gnathodiaphyseal dysplasia. Biochem. Biophys. Res. Commun. *357*, 126–132.

Nilius, B., Prenen, J., Szucs, G., Wei, L., Tanzi, F., Voets, T., and Droogmans, G. (1997). Calcium-activated chloride channels in bovine pulmonary artery endothelial cells. J. Physiol. *498*, 381–396.

Perez-Cornejo, P., De Santiago, J.A., and Arreola, J. (2004). Permeant anions control gating of calcium-dependent chloride channels. J. Membr. Biol. *198*, 125–133.

Pifferi, S., Pascarella, G., Boccaccio, A., Mazzatenta, A., Gustincich, S., Menini, A., and Zucchelli, S. (2006). Bestrophin-2 is a candidate calcium-activated chloride channel involved in olfactory transduction. Proc. Natl. Acad. Sci. USA *103*, 12929–12934.

Pusch, M. (2004). Ca(2+)-activated chloride channels go molecular. J. Gen. Physiol. *123*, 323–325.

Qu, Z., and Hartzell, H.C. (2000). Anion permeation in Ca(2+)-activated Cl(-) channels. J. Gen. Physiol. *116*, 825–844.

Ravin, N.V., Kuprianov, V.V., Gilcrease, E.B., and Casjens, S.R. (2003). Bidirectional replication from an internal ori site of the linear N15 plasmid prophage. Nucleic Acids Res. *31*, 6552–6560.

Rock, J.R., Futtner, C.R., and Harfe, B.D. (2008). The transmembrane protein TMEM16A is required for normal development of the murine trachea. Dev. Biol. *321*, 141–149.

Runft, L.L., Watras, J., and Jaffe, L.A. (1999). Calcium release at fertilization of Xenopus eggs requires type I IP(3) receptors, but not SH2 domain-mediated activation of PLCgamma or G(q)-mediated activation of PLCbeta. Dev. Biol. *214*, 399–411.

Samejima, M., and Sibaoka, T. (1982). Membrane potentials and resistances in excitable cells in the petiole and main pulvinus of *Mimosa pudica*. Plant Cell Physiol. *27*, 1081–1089.

Schaeren-Wiemers, N., and Gerfin-Moser, A. (1993). A single protocol to detect transcripts of various types and expression levels in neural tissue and cultured cells: In situ hybridization using digoxigenin-labelled cRNA probes. Histochemistry *100*, 431–440.

Sun, H., Tsunenari, T., Yau, K.W., and Nathans, J. (2002). The vitelliform macular dystrophy protein defines a new family of chloride channels. Proc. Natl. Acad. Sci. USA *99*, 4008–4013.

Takahashi, T., Neher, E., and Sakmann, B. (1987). Rat brain serotonin receptors in Xenopus oocytes are coupled by intracellular calcium to endogenous channels. Proc. Natl. Acad. Sci. USA *84*, 5063–5067.

Takizawa, P.A., DeRisi, J.L., Wilhelm, J.E., and Vale, R.D. (2000). Plasma membrane compartmentalization in yeast by messenger RNA transport and a septin diffusion barrier. Science *290*, 341–344.

Tarran, R., Button, B., and Boucher, R.C. (2006). Regulation of normal and cystic fibrosis airway surface liquid volume by phasic shear stress. Annu. Rev. Physiol. *68*, 543–561.

Tsien, R., and Pozzan, T. (1989). Measurement of cytosolic free Ca2+ with quin2. Methods Enzymol. *172*, 230–262.

Tsutsumi, S., Kamata, N., Vokes, T.J., Maruoka, Y., Nakakuki, K., Enomoto, S., Omura, K., Amagasa, T., Nagayama, M., Saito-Ohara, F., et al. (2004). The novel gene encoding a putative transmembrane protein is mutated in gnathodiaphyseal dysplasia (GDD). Am. J. Hum. Genet. *74*, 1255–1261.

West, R.B., Corless, C.L., Chen, X., Rubin, B.P., Subramanian, S., Montgomery, K., Zhu, S., Ball, C.A., Nielsen, T.O., Patel, R., et al. (2004). The novel marker, DOG1, is expressed ubiquitously in gastrointestinal stromal tumors irrespective of KIT or PDGFRA mutation status. Am. J. Pathol. *165*, 107–113.

Widdicombe, J.H. (2002). Regulation of the depth and composition of airway surface liquid. J. Anat. *201*, 313–318.

Yang, Y.D., Cho, H., Koo, J.Y., Tak, M.H., Cho, Y., Shim, W.S., Park, S.P., Lee, J., Lee, B., Kim, B.M., et al. (2008). TMEM16A confers receptor-activated calcium-dependent chloride conductance. Nature, in press. Published online August 24, 2008. 10.1038/nature07313.